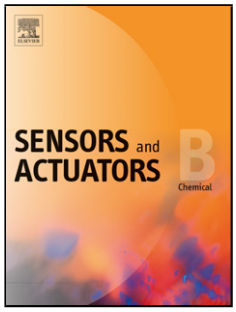

Title: An integrated optical Bragg grating refractometer for volatile organic compound detection

Author: Dominic J. Wales Richard M. Parker Priscilla Quainoo Peter A. Cooper James C. Gates Martin C. Grossel Peter G.R. Smith

PII: S0925-4005(16)30444-0
DOI: http://dx.doi.org/doi:10.1016/j.snb.2016.03.150
Reference: SNB 19955

To appear in: *Sensors and Actuators B*

Received date: 19-11-2015
Revised date: 21-3-2016
Accepted date: 28-3-2016

Please cite this article as: Dominic J.Wales, Richard M.Parker, Priscilla Quainoo, Peter A.Cooper, James C.Gates, Martin C.Grossel, Peter G.R.Smith, An integrated optical Bragg grating refractometer for volatile organic compound detection, Sensors and Actuators B: Chemical http://dx.doi.org/10.1016/j.snb.2016.03.150

An integrated optical Bragg grating refractometer for volatile organic compound detection

Dominic J. Wales[a,b] †, Richard M. Parker[a,b,1], Priscilla Quainoo[b], Peter A. Cooper[a], James C. Gates[a], Martin C. Grossel[b], Peter G. R. Smith[a]

[a]*Optoelectronics Research Centre, Faculty of Physical and Applied Sciences,* [b] *Department of Chemistry, Faculty of Natural and Environmental Sciences, University of Southampton, Southampton, United Kingdom, SO17 1BJ.*

† *Corresponding author; D.J.Wales@soton.ac.uk*

[1] Present address: Department of Chemistry, University of Cambridge, Cambridge, UK, CB2 1EW

Highlights:

- Describes an integrated optical Bragg grating sensor for volatile organic solvents.
- Reports real-time monitoring of a gas-flow, with on-chip temperature compensation.
- Distinct shifts in Bragg wavelength were measured upon exposure to a range of VOCs.
- The Bragg wavelength shift was correlated with analyte physicochemical properties.
- A linear QPSR model was developed to predict the sensor response to a VOC test set.

We report an integrated optical Bragg grating detector, fabricated using a direct UV-writing approach, that when coated with a thin-film of a hydrophobic siloxane co-polymer can perform as an all-optically accessed detector for hydrocarbon vapour. Upon exposure to a series of organic solvent vapours, both negative and positive Bragg wavelength shifts of differing magnitudes were measured. This was attributed to a combination of swelling and/or hydrocarbon solvent filling the free volume within the polymer film. A quantitative structural property relationship (QSPR) approach was utilised to create a multiple variable linear regression model, built from parameters that chemically described the hydrocarbons and the intermolecular interactions present between the co-polymer and hydrocarbon molecules. The resulting linear regression model indicated that the degree of swelling of the polysiloxane thin film when exposed to vapours of different hydrocarbons was due to the physico-chemical properties of the hydrocarbons and that this was the main causative factor of the measured Bragg wavelength shifts. Furthermore, this linear regression model allows for the prediction of the Bragg wavelength shift that would be measured upon exposure to vapours of another defined hydrocarbon. This detector is intrinsically safe in flammable environments. It includes on-chip thermal compensation, operates at telecoms wavelengths and has a predictable response to a variety of hydrocarbons making it ideal for detection of flammable hydrocarbon vapours in industrial and domestic processes.

Keywords: Bragg grating; refractive index sensor; volatile organic compound; integrated optics; polysiloxane.

1. Introduction

The detection of volatile organic compounds (VOCs), including hydrocarbons, is required to ensure legislative and safety targets are met in industrial environments. Hydrocarbon emission can occur on the large scale during industrial processes, and on the smaller scale in systems ranging from vehicles powered by combustion engines [1] to the use of adhesives and paints [2,3]. In situations such as industrial manufacturing plants that frequently contain explosive atmospheres it is a legal requirement that any measuring techniques be intrinsically spark-free [4].

One of the earliest devices for gaseous hydrocarbon detection was the 'Davy lamp', which revolutionised mining by allowing safe operation within potentially explosive environments [5]. More contemporarily, the most common portable detectors are Photo-Ionisation Devices (PIDs) [6]. Such detectors can achieve sub-ppm accuracy, but cannot provide continuous monitoring and the operator is exposed to potentially hazardous environments to take measurements [6]. Remote sensing can be achieved with other detection techniques, such as infrared open-path detection [7], however, this method can be cross-sensitive to dust clouds or vapour mists, which cause optical scattering losses and may lead to false positives. In contrast, optical fibre sensors do not suffer from optical power losses caused by dust and vapour mists, are intrinsically suitable for use in hazardous or explosive environments, and can be operated at standard telecoms wavelengths. Indeed, there are many examples in the literature of optical fibre gaseous hydrocarbon detectors and sensors, such as optical absorption-based sensors [8–11]. In contrast, relatively few examples of integrated optical sensors—planar lightwave circuits that contain several optical components which are combined to fulfil the sensing/detection function— have been reported for detection of hydrocarbons, despite the advantages of these over optical fibre-based sensors which include on-chip thermal compensation, the potential to combine multiple optical functions in a single device for multi-parameter analysis, [12,13] and the ability to remotely interrogate large multi-sensor arrays *via* optical fibre interconnects [14].

In the literature, hydrocarbon sensors have been modified with polymer thin-films that swell in the presence of hydrocarbon vapour, where the coupling of this swelling to electrochemical, mechanical or optical transduction technologies affords the output signal [15–21]. Thundat *et al*. reported a microring resonator integrated optical sensor, coated with a layer of poly(dimethylsiloxane) (PDMS). The PDMS swelled in the presence of

ethanol and acetone vapours, causing the thickness and permittivity of the layer to change which resulted in a shift of the measured resonant frequency [21]. Similarly, Lowe *et al*. utilised the swelling of polymer layers to develop a planar holographic sensor for a wide range of hydrocarbon vapours. The authors demonstrated that the holographic response, upon exposure to range of volatile organic compounds, could be explained by the Hildebrand solubility parameter in a non-linear manner [22]. Here, we investigate the efficacy of a polysiloxane layer as the active element in an integrated optical VOC detector with a diverse range of hydrocarbon solvents. The relationship between the refractive index of the swollen polymer layer with the properties of the solvents is probed by a quantitative structural property relationship (QSPR) linear regression model, enabling prediction of the sensor response to a test set of hydrocarbons.

2. Background

A Bragg grating is a periodic modulation of refractive index along a waveguiding channel, which in reflection acts as a wavelength-selective reflector. Bragg gratings are inherently sensitive to both temperature and strain, however if the light within the waveguide is able to interact with the local environment, then evanescent coupling allows for a measurable change in the optical characteristics [23]. Changes in this environment alter the effective refractive index, n_{eff} of the Bragg grating and result in a corresponding shift in the Bragg wavelength (λ_B). Here, an integrated optical refractometer (**Fig.S1a**) was fabricated by simultaneously 'writing' both the waveguide and Bragg gratings with a UV-laser directly into a planar photosensitised silica-on-silicon substrate, without the need for photolithographic processing [24–27]. Each Bragg grating functioned as an independent refractometer, capable of detecting changes in the refractive index near the surface *via* the corresponding spectral shift in the Bragg wavelength with sub-picometre precision (**Fig. S1b**). A thorough review of the fabrication of these planar integrated Bragg gratings devices using the direct UV-writing approach is given by Holmes *et al.* [28].

It has been shown previously that these devices are sensitive to physisorbed water on the surface of the exposed waveguides [29] and, upon functionalisation with a mesoporous aluminosilicate thin-film, they are capable of monitoring relative humidity in real-time [30]. Here we exploit the differing permeability of an amorphous polymer film to

hydrocarbon vapours to gain both sensitivity and specificity. Hydrocarbon vapours will solvate the polymer layer and the degree of solvation is specific to each analyte. This will determine the extent of swelling of the polymeric layer and consequently the measured refractive index of the polymer will change. It is noted that Hellmann *et al.* have reported a silica-on-silicon optical Bragg grating sensor for the detection of vapours of naphthalene, benzene, toluene and *m*-xylene, *via* a multi-layer film of γ-cyclodextrin [31,32]. However, the generalisability of their sensor is hindered by the limited host-guest selectivity of the γ-cyclodextrin macrocycle and the effect of binding constants was not discussed [33].

3. Results and Discussion

3.1. Integrated optical Bragg grating refractometer

An integrated optical Bragg grating device (BGD) comprising of a channel waveguide containing eight spectrally distinct Bragg gratings was fabricated (**Fig.1a**). The corresponding reflectance spectrum of the uncoated device is shown in **Fig.1b**, with a distinct spectral peak for each of the eight Bragg gratings. The central four Bragg gratings were designated for sensing, while the peripheral Bragg gratings (1540 nm and 1565 nm, marked with an asterisk in **Fig.1b**) were used for self-referencing against environmental fluctuations, principally temperature. The Bragg gratings at the extremities of the device (1535 and 1570 nm), while still suitable for temperature referencing, exhibited spectral fringes, due to interference effects, which degrade the quality of peak fitting. As such, these gratings were not used explicitly for referencing in the following work, but did allow for further confirmation of observed thermal trends.

The sensor region of the BGD was spin-coated with a thin-film of poly(hydroxymethyl–*co*–octylmethyl)siloxane (POHMS). As detailed in the Supplementary Information, POHMS was successfully synthesised *via* a hydrosilylation reaction with poly(hydroxymethyl)siloxane (PHMS). The resulting co-polymer contained 15 mol% of the octylmethyl monomer, as confirmed by NMR and FTIR spectroscopy. The differing hydrophobicity (corresponding to swelling ability [34]) of the two monomer components was anticipated to enable sensitivity to a wider range of solvent vapour than for a homogenous polymer. The refractive index of the co-polymer was measured as 1.4397 ± 0.0005 at 1553 nm wavelength (Metricon 2010/M prism coupling refractometer), with the film thickness approximately 1.4 μm as measured by scanning white light interferometry [35]. As the thickness of this polysiloxane film is expected to be far greater than the extent of the evanescent field of the guided optical mode

perpendicular to the surface of the device [36], any measured change in refractive index (after thermal compensation) should be exclusively due to solvent-triggered changes in the POHMS layer.

POSITION OF FIGURE 1(a) & (b)

3.2. Solvent vapour Sensing

The BGD was mounted within a gas flow cell and optically interrogated whilst exposed to either a flow of dry nitrogen carrier gas or a flow of nitrogen carrier gas saturated with solvent vapour, with the temperature independently monitored *via* a thermocouple. The carrier gas was enriched at a temperature 20 K higher than the boiling point of each solvent, with the flow cell being held at 301 K throughout. This gas sensing apparatus was based on previously reported organic vapour sensing experiments [37],[32] and the protocol is described in detail in the Supplementary Information and schematically in **Fig.S2**. The device was exposed to saturated vapour from a diverse set of fifteen solvents: methanol (MeOH, 19.3%), acetone (Acet., 34.2%), *n*-hexane (n-hex, 22.8%), isopropyl alcohol (IPA, 6.9%), dichloromethane (DCM, 63.7%), cyclohexane (CY, 14.6%), cyclohexene (CH, 13.3%), benzene (Benz.,14.3%), carbon disulfide (CS_2, 52.6%), ethyl acetate (EA, 14.2%), chloroform ($CHCl_3$, 29.4%), tetrahydrofuran (THF, 24.2%), toluene (Tol., 4.3%), oct-1-ene (O-1-E, 2.7%), 1,4-difluorobenzene (1,4-dfb, 9.7%) and water (H_2O, 3.7%). The reported proportion of each solvent dispersed in 100 % saturated nitrogen at 301 K is given in parenthesis above [38].

Upon exposure to solvent vapour, a measurable wavelength shift was recorded for all Bragg gratings. The average Bragg wavelength shifts for the four polysiloxane-covered Bragg gratings, $\lambda_{B(C)}$, and two uncovered, 'reference' Bragg gratings, $\lambda_{B(U)}$, were calculated for each solvent and defined as the differential from the Bragg wavelength in a dry nitrogen atmosphere at 301 K (**Fig.S3**). It was determined that there was no correlation between the proportion of each solvent analyte in saturated nitrogen at 301 K and the corresponding values of $\Delta\lambda_{B(U)}$ or $\Delta\lambda_{B(C)}$, for each solvent analyte. (**Fig.S4**).

The average $\Delta\lambda_{B(U)}$ values are plotted against the analyte refractive index in **Fig.2a**. For all solvents $\Delta\lambda_{B(U)}$ reported a small but positive wavelength shift, however there is no correlation

with the refractive index of the solvent potentially condensing on the sensor surface. This shift is instead explained by the more significant jump in temperature upon flowing saturated vapour over the device. The correlation between temperature and $\Delta\lambda_{B(U)}$ is exemplified in **Fig.2b** for an exposure cycle to toluene vapour. The temperature within the flow cell, as measured by the thermocouple, increased by 3 °C during solvent exposure after which it returned to the initial value. This trend is replicated by the two uncovered gratings, with the magnitude of the shift consistent with the thermo-optic properties of the BGD [12]. This relationship is similarly observed for all solvents, with $\Delta\lambda_{B(U)}$ partially correlated to a function of both (solvent boiling point + 20) / K and the maximum absolute temperature measured within the cell during a solvent exposure event (**Fig.S5a & b**). It must be noted that the absolute temperature of the device will differ from the absolute temperature of the gas flow within the cell (as measure by the thermocouple), however it confirms the efficacy of the uncovered Bragg gratings for *in situ* thermal compensation.

POSITION OF FIGURE 2(a) & (b)

In stark contrast with the behaviour of the uncovered Bragg gratings, exposure to the series of hydrocarbons resulted in both positive and negative wavelength shifts of $\Delta\lambda_{B(C)}$, relative to the dry nitrogen flow. Temperature (and strain) effects were removed by subtraction of the corresponding $\Delta\lambda_{B(U)}$ measurement from $\Delta\lambda_{B(C)}$ for each solvent. The referenced Bragg wavelength shifts of the POHMS-covered Bragg gratings $\delta(\Delta\lambda_B)$ are shown below in **Fig.S6**. If solvent ingress into the free volume of the polysiloxane layer was the dominant factor, it would be expected that $\delta(\Delta\lambda_B)$ would be both positive for all solvents and correlate with the trend in refractive index. **Fig.3** does show correlation with refractive index, with the exception of carbon disulfide and water, but with a significant offset from the initial polymer state. It is known that both PDMS and PHMS swell in the presence of solvent vapour [39,40]; therefore it is expected that solvent vapour will swell the POHMS film employed here, with the extent of swelling being dependent on the solvent. Swelling has two components: (i) solvent molecules displace the nitrogen gas in the free volume between polymer chains; and (ii) the thickness of the thin film will increase, lowering the density. With respect to $\delta(\Delta\lambda_B)$, factor (i) would increase the Bragg wavelength, whereas (ii) would inversely lower it. The relative significance of factors (i) and (ii) are expected to be highly solvent dependent. For example, $\delta(\Delta\lambda_B)$ for all the solvents which contain a hydrocarbon moiety (e.g. ≡CH, $=CH_2$ or

-CH_3) correlate with the refractive index of the analyte solvent, but for water and carbon disulfide, solvents which do not include a hydrocarbon moiety, the Bragg shift does not correlate with the refractive index. This suggests that the magnitudes of (i) and (ii) are dependent on whether that particular solvent molecule is 'good' or 'poor' at solvating the POHMS layer.

POSITION OF FIGURE 3

An increase in refractive index would be caused by factor (i)—the more solvent molecules between the polymer chains, the greater the refractive index. However, another property is needed to give some measure of (ii). Therefore, in a further attempt to determine which solvents were 'good', or 'poor', the correlation between values of $\delta(\Delta\lambda_B)$ and the Hildebrand solubility parameter, δ_H, was investigated. The Hildebrand solubility parameter is a descriptor commonly used to describe the intermolecular forces, excluding hydrogen bonding [41], between the molecules of a solvent, and thus the ability of the solvent to solvate polymers. **Fig.4** shows δ_H plotted against $\delta(\Delta\lambda_B)$, for all non-hydrogen bonding solvents. Information on how the δ_H values for the solvents were obtained or calculated is given in the Supplementary Information. It was found that the relationship between δ_H and $\delta(\Delta\lambda_B)$ was complex with asymptotic behaviour around $\delta_H \approx 18.5$ $MPa^{1/2}$. The overall shape of the plot, and asymptotic behaviour, corroborates the work of Lowe *et al.* [22]. However, there were three significant outliers that are circled in red in **Fig.4**. Carbon disulfide can be discounted on the basis that it does not contain C-H bonds; all the other analytes contain C-H bonds. Ethyl acetate and dichloromethane can be explained by their comparatively high relative polarities; polarity affects the solvating power of a solvent in a manner that is not fully taken into account by the Hildebrand solubility parameter [42]. Benzene (δ_H = 18.8 $MPa^{1/2}$) and toluene (δ_H = 18.2 $MPa^{1/2}$) demonstrated the largest magnitude positive Bragg wavelength shifts. This suggests that the δ_H value of our POHMS layer is approx. 18.5 $MPa^{1/2}$; compounds with very similar δ_H values will readily dissolve in one another, which is consistent with the use of toluene as the reaction solvent for the post-functionalisation of PHMS.

POSITION OF FIGURE 4

3.3 Building the QSPR model

The relationships between $\delta(\Delta\lambda_B)$ and either the solvent refractive index or the Hildebrand solubility parameter were non-linear and as such are inherently impractical for facilitating prediction of measured Bragg wavelength shifts. In addition, the relationship between δ_H and $\delta(\Delta\lambda_B)$ were only correlated for non-hydrogen bonding solvents, leaving several solvents unaccounted for. This warranted further investigation into which properties of the solvents were affecting the values of $\delta(\Delta\lambda_B)$ and ultimately to determine a linear relationship to facilitate prediction. Therefore, a QSPR study was performed. This approach enabled the determination of the physico-chemical parameters of the solvents under study, as detailed in **Table 1**, which had the most significant effect on $\delta(\Delta\lambda_B)$ and thus the largest contribution to polymer solvation and/or swelling.

Chemical descriptors (1) to (6) were selected as the magnitudes of these descriptors which depend on, or influence, the strength of the intermolecular forces between the molecules of a solvent. Descriptor (7) was chosen because refractive index is the main physico-chemical property that is being investigated in this work. Chemical descriptors (8) to (12) were chosen as these describe the functional groups present, the overall structure of the solvent molecules, how this impacts on the steric bulk of the solvent molecules, and on the intermolecular forces between the solvent molecules.

Before the QSPR model was constructed, the order of the solvents was randomized and three solvents were arbitrarily selected, removed and labelled as the ‘test set’: ethyl acetate (EA), carbon disulfide (CS2) and oct-1-ene (O-1-E). The remaining twelve solvents were labelled as the ‘training set’. Next, the coefficient of variation (CV) was calculated as a measure of the spread in the data — if CV tends towards zero, then this indicates that there is little or no spread in the set of data and consequentially is not suitable to be included in the regression model. The absolute magnitudes of CV for the descriptors are given in **Table 2**.

The magnitude of the coefficient of variation of the two descriptors, 'boiling point' and 'refractive index', were the smallest and near zero and consequentially these were removed from the QSPR model. Descriptors with small magnitude values of the coefficient of variation (CV) that are near zero, possess little or no spread. Any variable that has a CV with little or no spread will have little to no effect on the regression model. Therefore, refractive index was removed, despite the correlation with $\Delta\Delta\lambda_B$ as shown in **Fig.3** above. The values of the remaining descriptors were then scaled using the autoscaling method [66]. Pairwise correlations between the chemical descriptors were checked by creating a correlation matrix, as reported in **Table 3.** The Hildebrand solubility parameter, molecular weight, total polarisable surface area and number of hydrogen bond donor groups were subsequently removed from the QSPR model building process as these descriptors had very significant anti–correlation or correlation (|0.70| < absolute magnitude of correlation coefficient) with at least two other descriptors—significant correlation or anti-correlation can influence the statistics that describe the regression models. Based on this, the Hildebrand solubility parameter was removed, despite the correlation with $\Delta\Delta\lambda_B$ as shown in **Fig.4**. Six descriptors then remained in the QSPR model building process.

The QSPR model was derived with multiple successive multiple linear regressions of the data. At first, all six remaining chemical descriptors were included and a multiple linear regression was performed. The p–value (which is linked to the t–statistic) was visually inspected and the descriptor with largest p–value was deemed the least significant and thus removed. The multiple linear regression was performed again with the remaining five descriptors and the chemical descriptor now with the largest magnitude p–value discarded. This process of backward step regression model building [67] was continued until only three chemical descriptors remained. The derived regression model equation was then given by:

$$Predicted\ \delta(\Delta\lambda_B) = (-34.21 \times Log_{10}K_{OW}) - (65.11 \times nHbA) + (103.15 \times RDBE) + 25.44$$

Eq.1

where *nHbA* is the number of hydrogen bond acceptors and *RDBE* is ring double bond equivalents. It should be noted that the predicted $\delta(\Delta\lambda_B)$ values are unitless due to the autoscaling step. The predicted values of $\delta(\Delta\lambda_B)$, were calculated using **Eqn.1** and plotted against the magnitudes of the experimental $\delta(\Delta\lambda_B)$ values, as shown in **Fig.5**. The R^2 coefficient for this regression model was 0.94. The R^2 coefficient is a definition of how well a regression model describes the variation in the observed experimental values, where a value of 1 corresponds to perfect correlation [67]. Thus the model is reasonably robust as it moderately correlates to the training set data and explains the change in experimental $\delta(\Delta\lambda_B)$ values upon exposure of the sensor device to different solvent vapours. However, there are sources of uncertainty such as in the experimental values of $\log_{10}K_{OW}$ (taken from the literature) and including the weak hydrogen-bond acceptor groups in both 1,4-dfb and CS2 when calculating values of *nHbA.*

POSITION OF FIGURE 5

3.4 Testing the QSPR model

The QSPR model was tested by using **Eq.1** to predict the $\delta(\Delta\lambda_B)$ values that correspond to the three 'test' solvents. The predicted values of $\delta(\Delta\lambda_B)$ for the test solvents are plotted in red in **Fig.5,** it can be seen that the predicted values of $\delta(\Delta\lambda_B)$ for the test set correlate with the trend in $\delta(\Delta\lambda_B)$ from the training set. However, to quantitatively test the model, the predictive power of the model was determined by calculation of the Q^2 value; where a value of zero shows no predictive ability in the model whereas a value of one shows perfect predictive ability [68]. Performing this calculation yielded a Q^2 value of 0.68. Values of $Q^2 > 0.50$ are generally accepted as a measure of significant predictive ability of a regression model [68].

To further test the robustness of the regression model, the similarity of the training set solvents was measured, in terms of the three key descriptors in **Eq.1**, following the method described by Willet [69]. The diversity of the set of solvents was ~1 – i.e. there was no similarity between the solvents. This result is important as it shows that the linear regression model was built on a very diverse set of analytes and thus is both widely applicable and robust. This suggests that the values of $R^2 = 0.93$ and the $Q^2 = 0.68$ for this model are even more significant than implied above – it is typically harder to achieve a model with significant fit to a diverse set of molecules than to a set of similar molecules.

3.5 Detector response time

The response time of a gas sensor is defined as the time taken to achieve 90 % of the final stable change of a sensor after a step increase of the concentration of the analyte gas [30,70].The response time of the BGD within the flow system was determined from three independent sensing events, during which the flow system was switched from dry nitrogen gas to a saturated toluene vapour. Starting from a stable baseline value in dry nitrogen, the time taken for a stable Bragg wavelength shift to occur when exposed to the saturated vapour was recorded at 301 K (**Fig.6**). For this iteration of the sensor device, 90 % of the final constant Bragg wavelength shift (t_{90}) was reached in ~100 s, with the grating sampling rate set to 20 s for all experiments. This response time is comparable to the microwave ring resonator sensor reported by Thundat *et al.* [21], but slower by one order of magnitude than the holographic sensor device reported by Lowe *et al.*, the response time of which, for a 0 – 100 % change in concentration of the vapour analyte, is ~ 8 s [22]. It is proposed that the response time is both diffusion and transport limited. There was a difference in the response time for different solvents of different solubilising power—for toluene the response time was ~100 s and for water ~ 600 s. This is attributed to different rates of diffusion into the hydrophobic POHMS and consequentially a thinner film would significantly shorten t_{90}. However, it should be noted that neither the thermocouple response nor the uncovered 'reference' gratings show an instantaneous increase upon exposure to solvent vapour (**Fig.2b**) and as such, the rate of gas transport may also contribute significantly to the measured response time. With improved engineering of the flow cell, the effect of rate of gas transport could be potentially negated.

POSITION OF FIGURE 6

4. Conclusions

It has been demonstrated that an integrated optical Bragg grating device, fabricated using the direct UV-writing approach, can be modified with a poly(hydroxymethyl–*co*–octylmethyl)siloxane thin film, that contained 15 mol% of the octylmethyl monomer, to detect the presence of hydrocarbon vapours. For a series of diverse hydrocarbons and water, both negative and positive Bragg wavelength shifts of differing magnitudes were measured. Upon investigation into the sensing mechanism, it was revealed that the Bragg wavelength shift was to the result of the solubility of the polysiloxane film in the solvent vapour; this was quantified through the use of Hildebrand solubility parameter. The study of the interaction of solvent vapour with thin films is important for applications such as photolithography and

separation membrane fabrication/science [71], our device could be employed to study such interactions or to screen new polymer films.

The POHMS thin film was robust to repeated exposures to a wide range of solvents, with no degradation caused by solubilisation being observed, as evidenced by a return to the initial Bragg wavelength between each solvent exposure cycles. The composition of the POHMS thin film was not optimised, and it is expected that the sensitivity and selectivity will improve by tuning the thickness and composition of the polysiloxane layer. For example, a more hydrophobic polysiloxane is expected to swell further in the presence of hydrophobic solvents. Furthermore, by multiplexing polysiloxane films of differing hydrophobicities, it is expected that further elucidation of the nature and abundance of each vapour will be possible by differential analysis. This could be further combined with previously reported methods for continuous tracking of relative humidity [30], temperature [12], pressure [72], or chemo/bio-detection [73] on a single BGD within a distributed optical fibre-based sensor network.

A QSPR approach was utilised to create a multiple variable linear regression model, built from parameters that chemically described the solvents. The resulting linear regression model further confirmed that the solubility of the thin film of polysiloxane in the different solvents arose from the inherent properties of the solvent and that this was the main cause of the Bragg wavelength shifts measured. Additionally, this linear regression model equation allowed for the prediction of the Bragg wavelength shift that would be measured with this iteration of the BGD for any given solvent with known values of: $\log_{10}K_{OW;}$ the number of ‘hydrogen bond acceptors’; and number of ‘ring and double bond equivalents’. The values for these properties are readily available in the literature or can be calculated (e.g. molinspiration software [63]). The facile fabrication techniques and associated advantages of the planar integrated optical format makes this sensor device, when modified with a thin film of poly(hydroxymethyl–*co*–octylmethyl)siloxane, a viable organic vapour detector that offers advantages over current electrical devices in a range of domestic, commercial and industrial settings.

5. Acknowledgements

This work was supported by the UK Engineering Physical Sciences Research Council (EPSRC DTG: EP/P505119/1) and the ISCE-Chem project (No. 4061) which was co-financed by the European Regional Development Fund (ERDF) through the INTERREG IV A France (Channel) - England cross-border cooperation Programme. RMP acknowledges the EPSRC for a Ph.D. Plus Fellowship (EPSRC: EP/P505739/1). PQ was an undergraduate Chemistry student during this project. PAC acknowledges the EPSRC for doctoral training funding. Open access data for this work can be found at http://dx.doi.org/10.5258/SOTON/384402.

References

[1] A.W. Reitze, Air Pollution Control Law: Compliance and Enforcement, Environmental Law Institute, Washington, 2001.

[2] C.F. Murphy, D.T. Allen, Hydrocarbon emissions from industrial release events in the Houston-Galveston area and their impact on ozone formation, Atmos. Environ. 39 (2005) 3785–3798.

[3] V. Brown, Determination of aromatic hydrocarbon emissions from paint and related products by an impinger method, Environ. Int. 16 (1990) 283–289.

[4] Directive 94/9/EC of the European Parliament and the Council of 23 March 1994 on the approximation of the laws of the Member States concerning equipment and protective systems intended for use in potentially explosive atmospheres, European Parliament and Council, 1994.

[5] H. Davy, On the Fire-Damp of Coal Mines, and on Methods of Lighting the Mines So as to Prevent Its Explosion, Phil. Trans. R. Soc. Lond. 106 (1816) 1–22.

[6] G. Manes, G. Collodi, R. Fusco, L. Gelpi, A. Manes, A Wireless Sensor Network for Precise Volatile Organic Compound Monitoring, Int. J. Distrib. Sens. Networks. 2012 (2012) 13.

[7] D.P. Nolan, Handbook of Fire and Explosion Protection Engineering Principles: For Oil, Gas, Chemical and Related Facilities, 3rd ed., Elsevier Science Ltd, 2014.

[8] O.S. Wolfbeis, Fibre-optic chemical sensors and biosensors, Anal. Chem. 74 (2002) 2663–2677.

[9] O.S. Wolfbeis, Fibre-optic chemical sensors and biosensors, Anal. Chem. 78 (2006) 3859–74.

[10] O.S. Wolfbeis, Fiber-optic chemical sensors and biosensors., Anal. Chem. 80 (2008) 4269–83.

[11] X.-D. Wang, O.S. Wolfbeis, Fiber-optic chemical sensors and biosensors (2008-2012)., Anal. Chem. 85 (2013) 487–508.

[12] R.M. Parker, J.C. Gates, M.C. Grossel, P.G.R. Smith, A temperature-insensitive Bragg grating sensor—Using orthogonal polarisation modes for in situ temperature compensation, Sensors Actuators B Chem. 145 (2010) 428–432.

[13] L.A. Coldren, S.W. Corzine, M.L. Masanovic, Diode Lasers and Photonic Integrated Circuits, 2nd Editio, John Wiley & Sons, New Jersey, 2012.

[14] J. Janata, Principles of Chemical Sensors, Springer Science + Business Media, New York, 2009.

[15] M.A. Urbiztondo, A. Peralta, I. Pellejero, J. Sesé, M.P. Pina, I. Dufour, et al., Detection of organic vapours with Si cantilevers coated with inorganic (zeolites) or organic (polymer) layers, Sensors Actuators B Chem. 171-172 (2012) 822–831.

[16] A. Mirmohseni, H. Abdollahi, K. Rostamizadeh, Analysis of transient response of single quartz crystal nanobalance for determination of volatile organic compounds, Sensors Actuators B. Chem. 121 (2007) 365–371.

[17] L. Silva, T. Rochasantos, A. Duarte, Development of a fluorosiloxane polymer-coated optical fibre sensor for detection of organic volatile compounds, Sensors Actuators B Chem. 132 (2008) 280–289.

[18] B.K. Lavine, N. Kaval, D.J. Westover, L. Oxenford, New Approaches to Chemical Sensing-Sensors Based on Polymer Swelling, Anal. Lett. 39 (2006) 1773–1783.

[19] U. Altenberend, A. Oprea, N. Barsan, U. Weimar, Contribution of polymeric swelling to the overall response of capacitive gas sensors., Anal. Bioanal. Chem. 405 (2013) 6445–52.

[20] R. Pernice, G. Adamo, S. Stivala, A. Parisi, A.C. Busacca, D. Spigolon, et al., Opals infiltrated with a stimuli-responsive hydrogel for ethanol vapor sensing, Opt. Mater. Express. 3 (2013) 1820.

[21] A. Sohrabi, P. Mojir Shaibani, M.H. Zarifi, M. Daneshmand, T. Thundat, A novel technique for rapid vapor detection using swelling polymer covered microstrip ring resonator, in: 2014 IEEE MTT-S Int. Microw. Symp., IEEE, 2014: pp. 1–4.

[22] J.L. Martínez-Hurtado, C.A.B. Davidson, J. Blyth, C.R. Lowe, Holographic Detection of Hydrocarbon Gases and Other Volatile Organic Compounds, Langmuir. 26 (2010) 15694–15699.

[23] I.J.G. Sparrow, G.D. Emmerson, C.B.E. Gawith, P.G.R. Smith, M. Kaczmarek, A. Dyadyusha, First order phase change detection using planar waveguide Bragg grating refractometer, Appl. Phys. B. 81 (2005) 1–4.

[24] M. Olivero, M. Svalgaard, Direct UV-written broadband directional planar waveguide couplers, Opt. Express. 13 (2005) 8390.

[25] D.O. Kundys, J.C. Gates, S. Dasgupta, C. Gawith, P. Smith, Use of Cross-Couplers to Decrease Size of UV Written Photonic Circuits, IEEE Photonics Technol. Lett. 21 (2009) 947–949.

[26] G.D. Emmerson, S.P. Watts, C.B.E. Gawith, V. Albanis, M. Ibsen, R.B. Williams, et al., Fabrication of directly UV-written channel waveguides with simultaneously defined integral Bragg gratings, Electron. Lett. 38 (2002) 1531–1532.

[27] C.B.E. Gawith, G.D. Emmerson, S.G. McMeekin, J.R. Bonar, R.I. Laming, R.B. Williams, et al., Small-spot interference pattern for single-step 2D integration and wide wavelength detuning of planar Bragg gratings, Electron. Lett. 39 (2003) 1050.

[28] C. Holmes, J.C. Gates, L.G. Carpenter, H.L. Rogers, R.M. Parker, P.A. Cooper, et al., Direct UV-written planar Bragg grating sensors, Meas. Sci. Technol. 26 (2015) 112001.

[29] I. Sparrow, G. Emmerson, C. Gawith, P. Smith, Planar waveguide hygrometer and state sensor demonstrating supercooled water recognition, Sensors Actuators B Chem. 107 (2005) 856–860.

[30] D.J. Wales, R.M. Parker, J.C. Gates, P.G.R. Smith, M.C. Grossel, An Investigation into Relative Humidity Measurement using an Aluminosilicate Sol-gel Thin Film as the Active layer in an Integrated Optical Bragg grating Refractometer, Sensors Actuators B Chem. 188 (2013) 857–866.

[31] M. Girschikofsky, M. Rosenberger, S. Belle, M. Brutschy, S.R. Waldvogel, R. Hellmann, Highly Sensitive Detection of Naphthalene in Solvent Vapor Using a Functionalized PBG Refractive Index Sensor, Sensors. 12 (2012) 2018–2025.

[32] M. Girschikofsky, M. Rosenberger, S. Belle, M. Brutschy, S.R. Waldvogel, R. Hellmann, Optical planar Bragg grating sensor for real-time detection of benzene, toluene and xylene in solvent vapour, Sensors Actuators B Chem. 171-172 (2012) 338–342.

[33] J.W. Steed, J.L. Atwood, Supramolecular Chemistry, 2nd ed., Wiley, Chichester, 2009.

[34] S. Guizzetti, M. Benaglia, J.S. Siegel, Poly(methylhydrosiloxane)-supported chiral

imidazolinones: a new versatile, highly efficient and recyclable organocatalysts for stereoselective Diers-Alder cycloaddition reactions, Chem. Comm. 48 (2012) 3188–3190.

[35] S. Wood, Understanding scanning white light interferometry, MICROmanfacturing. (2009) 19–21,47.

[36] D.J. Wales, Planar Integrated Optical Bragg Grating Gas Sensors, Ph.D. Thesis, University of Southampton, 2013.

[37] L.I.B. Silva, T.A.P. Rocha-Santos, A.C. Duarte, Sensing of volatile organic compounds in indoor atmosphere and confined areas of industrial environments., Glob. NEST J. 10 (2008) 217–225.

[38] R.C. Weast, M.J. Astle, eds., Handbook of Chemistry and Physics, 60th ed., Chemical Rubber Publishing Company, Boca Raton, 1980.

[39] J.N. Lee, C. Park, G.M. Whitesides, Solvent compatibility of poly(dimethylsiloxane)-based microfluidic devices., Anal. Chem. 75 (2003) 6544–54.

[40] S. Guizzetti, M. Benaglia, J.S. Siegel, Poly(methylhydrosiloxane)-supported chiral imidazolinones: new versatile, highly efficient and recyclable organocatalysts for stereoselective Diels-Alder cycloaddition reactions., Chem. Comm. 48 (2012) 3188–3190.

[41] B.A. Miller-Chou, J.L. Koenig, A Review of Polymer Dissolution, Prog. Polym. Sci. 28 (2003) 1223–1270.

[42] J. Burke, Solubility Parameters: Theory and Application, in: B. Pap. Gr. Annu. Vol. Three, CoOL, 1984.

[43] A. Villares, B. Giner, H. Artigas, C. Lafuente, F.M. Royo, Study of the surface tensions of cyclohexane or methylcyclohexane with some cyclic ethers, J. Solution Chem. 34 (2005) 185–198.

[44] C. Bermuidez-Salguero, A. Amigo, J. Gracia-Fadrique, Surface tension data of aqueous binary mixtures of methyl, ethyl, propyl & butyl acetates at 298.15 K, J. Chem. Eng. Data. 55 (2010) 2905–2908.

[45] J.E. Shewmaker, C.E. Vogler, E. Roger Washburn, Spreading of hydrocarbons and related compounds on water, J. Phys. Chem. 58 (1954) 945–947.

[46] J. Koefoed, J.V. Villadsen, Surface tension of liquid mixtures. A micro-method applied to the systems: chloroform-carbon tetrachloride, benzene-diphenylmethane and heptane-hexadecane., Acta Chem. Scand. 12 (1958) 1124–1126.

[47] H.M. Trimble, The variation of the capillary action of solution with time, J. Phys. Chem. 32 (1928) 1211.

[48] W.F. Seyer, E.G. King, Systems of sulfur dioxide and hydrogen derivatives of benzene, J. Am. Chem. Soc. 55 (1933) 3140–3144.

[49] E. Jimenez, H. Casas, L. Segade, C. Franjo, Surface tensions, refractive indexes & excess molar volumes of hexane + 1-alkanol mixtures at 298.15 K, J. Chem. Eng. Data. 45 (2000) 862–866.

[50] I.L. Acevedo, G.C. Pedrosa, M. Katz, Internal pressure & cohesive energy density for binary non-electrolyte mixtures, J. Solution Chem. 9 (1990) 911–921.

[51] J. Aracil, G. Luengo, B.S. Almeida, M.M.T. da Gama, R.G. Rubio, M.D. Pena, Surface properties of mixtures of molecular fluids: An experimental and theoretical study of carbon disulfide + dichloromethane and carbon disulfide + carbon tetrachloride, J. Phys. Chem. 93 (1989) 3210–3218.

[52] J.L. Zurita, M.L.G. de Soria, M.A. Postigo, M. Katz, Excess thermodynamic properties of the 2-propanol + dichloromethane system at 25 oC, J. Solution Chem. 16 (1987) 163–170.

[53] R.S. Myers, B.A. Berenbach, H.L. Clever, Surface tension of p-diflurobenzene, hexafluorobenzene and some p-difluorobenzene - p-xylene solutions, J. Chem. Eng. Data. 14 (1969) 91.

[54] A. Ahosseini, B. Sensenich, L.R. Weatherley, A.M. Scurto, Phase equilibrium, volumetric and interfacial properties of the ionic liquid, 1-hexyl-3 methyl imidazolium Bis(trifluoromethylsulfonyl)amide and 1-octene, J. Chem. Eng. Data. 55 (2010) 1611–1617.

[55] M. Hadded, A. Mayaffre, P. Letellier, Tension superficelles des solutions ideales: Application aux solvants binaries constitutes de methanol et de nitrate d'ethylammonium fondu a 298 K, J. Chim. Phys. Physico-Chimie Biol. 86 (1989) 525–538.

[56] L.F. Transue, E. Roger Washburn, F.H. Kahler, The direct measurement of the spreading pressures of volatile organic liquids on water, J. Am. Chem. Soc. 64 (1942) 274.

[57] Sigma-Aldrich, United Kingdom | Sigma-Aldrich, (2013). http://www.sigmaaldrich.com/united-kingdom.html (accessed August 12, 2013).

[58] J.-L.M. Abboud, R. Notario, Critical compilation of scales of solvent parameters. Part I. Pure, non-hydrogen bond donor solvents, Pure Appl. Chem. 71 (1999) 645–718.

[59] V. Svoboda, V. Charvátová, V. Majer, V. Hynek, Determination of heats of vaporization and some other thermodynamic properties for four substituted hydrocarbons, Collect. Czechoslov. Chem. Commun. 47 (1982) 543–549.

[60] G. Liesmann, W. Schmidt, Recommended Thermophysical Data, in: Data Compil. Saechsische Olefin. Boehlen Ger., 1995.

[61] J. Sangster, LOGKOW © A database of evaluated octanol-water partition coefficients (LogP), LOGKOW - Sangster Res. Lab. (2013). http://logkow.cisti.nrc.ca/logkow/ (accessed August 3, 2013).

[62] R.E. Sah, J. Zhang, J.M. Deen, J. Yota, A. Toriumi, Silicon Nitride, Silicon Dioxide, and Emerging Dielectrics, ECS Trans. 19 (2009) 467–477.

[63] Molinspiration Cheminformatics, Molinspiration Cheminformatics: Cheminformatics on the web, (2013). http://www.molinspiration.com/ (accessed August 12, 2013).

[64] A.B. Sannigrahi, A.K. Chandra, Hydrogen Bonding between Phenols and Carbon Disulphide, Bull. Chem. Soc. Jpn. 40 (1967) 1344–1349.

[65] P.C. Singh, M. Ray, G.N. Patwari, Theoretical Investigation of In-Plane Hydrogen-Bonded Complexes of Ammonia with Partially Substituted Fluorobenzenes, J. Phys. Chem. A. 111 (2007) 2772–2777.

[66] K. Varmuza, P. Filzmoser, Introduction to Multivariate Statistical Analysis in Chemometrics, 1st ed., CRC Press, Boca Raton, 2009.

[67] A.R. Leach, V.J. Gillet, An Introduction to Chemoinformatics, Kluwer Academic Publishers, Dordrecht, 2003.

[68] R. Carbo-Dorca, R. Carbo, D. Robert, L. Amat, X. Girones, E. Besalu, Molecular

Quantum Similarity in QSAR and Drug Design, Springer UK, 2000.

[69] P. Willet, Molecular Diversity Techniques for Chemical Databases, Inf. Res. 2 (1996) Paper 19.

[70] M.E. Azim-Araghi, A. Krier, Thin film (ClAlPc) phthalocyanine gas sensors, in: S.M. Vaezi-Nejad (Ed.), Sel. Top. Adv. Solid State Fibre Opt. Sensors, IET, 2000: pp. 215–243.

[71] G.J. Price, J.M. Buley, A Quartz Crystal Microbalance Apparatus for Studying Interactions of Solvents with Thin Polymer Films, Progess Org. Coatings. 19 (1991) 265–274.

[72] C. Holmes, L.G. Carpenter, J.C. Gates, P.G.R. Smith, Miniaturization of Bragg-multiplexed membrane transducers, J. Micromechanics Microengineering. 22 (2012) 025017.

[73] R.M. Parker, D.J. Wales, J.C. Gates, J.G. Frey, P.G.R. Smith, M.C. Grossel, Monolayer detection of ion binding at a crown ether-functionalised supramolecular surface via an integrated optical Bragg grating, Analyst. 139 (2014) 2774–2782.

Biographies

Dominic J. Wales is currently a Research Fellow in the Department of Chemistry at the University of Southampton (UK) working on amphiphilic self-assembling supramolecular lanthanide complexes for Langmuir-Blodgett applications and for gas sensing. He graduated from the University of Southampton (UK) with a 1st Class MChem degree in Chemistry in 2009. In collaboration with the Optoelectronics Research Centre, his Ph.D. thesis investigated the application of porous materials and polymers to integrated optical refractometers for application in gas sensing. After completion of his Ph.D. studies in 2013, he continued researching in the fields of gas sensing, metal-organic framework chemistry and zeolite chemistry as a Research Officer at the University of Bath (UK).

Richard M. Parker graduated from the University of Southampton (UK) with a MChem degree in 2007, followed by the award of a Ph.D. in chemistry in 2011. In collaboration with the Optoelectronics Research Centre, his Ph.D. thesis investigated the application of supramolecular and surface chemistry to an integrated optical refractometer for application in chemical sensing. After completion of his doctoral studies in 2010, he continued researching in the fields of optical sensors, fibre optics and supramolecular chemistry at the University of Southampton until 2012. He is currently a Postdoctoral Research Associate at the University of Cambridge (UK).

Priscilla Quainoo was an undergraduate MChem Chemistry student in the School of Chemistry at the University of Southampton (UK) during this work.

Peter A. Cooper was a Ph.D. student at the Optoelectronics Research Centre at the University of Southampton (UK) during this work. His undergraduate degree was in physics from the University of Edinburgh (UK). Prior to his Ph.D. he worked for a company producing optical lenses and mirrors using CNC polishing machines. He is investigating micro milling using diamond tools to produce new optical structures for integrated optics and MEMs. He has published two journal papers as part of his Ph.D. describing new MOEM devices.

James C. Gates is currently a senior research fellow at the Optoelectronics Research Centre (ORC) at the University of Southampton (UK). He gained an MPhys degree from the University of Southampton (UK) in 1999, and completed his PhD at the ORC in 2003. He

continued researching in the field of nanophotonics in the Physics department at the University of Southampton (UK) before returning to the ORC in 2006. He has published over 50 journal papers and 120 conference publications in the areas of optical sensing, integrated optics, optical fabrication and quantum technology.

Martin C. Grossel is Emeritus Fellow in Organic Chemistry at the University of Southampton (UK) where he has worked since 1991 and Emeritus Student and Lecturer in Organic Chemistry at Christ Church, University of Oxford (UK), where he has been a Tutor since 1973. He graduated from King's College, University of London, (UK) with a BSc in 1970 and a PhD in Physical Organic Chemistry in 1974. He has published over 90 journal papers together with books, reviews and patents. His research interests have focussed on conformational analysis of small organic molecules, organic molecular electronics, crystal engineering and applications of photoactive polymers and dendrimers within the fields of medicine, optoelectronics and materials science.

Peter G.R. Smith is a Professor at the Optoelectronics Research Centre and Associate Pro Vice-Chancellor International in the Faculty of Physical Sciences and Engineering at the University of Southampton (UK). He leads a research group concentrating on the fabrication of optical devices using integrated optics technology:- particularly on direct UV writing and precision machining of optical materials. He also works on periodic poling technology and nonlinear optics. He has over 200 publications, 10 patents and was the founder of two spin-outs from Southampton - Stratophase Ltd in 2003 and Covesion Limited in 2009.

Figure captions

Fig.1: (a) A schematic of the planar integrated Bragg grating hygrometer, illustrating the location of the eight Bragg gratings along the waveguide and the approximate peak Bragg wavelength in nanometres. The light grey region designates the thin polysiloxane film. The fibre-based optical interrogation system (in the dashed box) is connected to the chip using an optical fibre and is robustly pigtailed using standard telecomm assembly techniques. The reference Bragg gratings used (1540 nm and 1565 nm) are marked with an asterisk. **(b)** The corresponding reflected Bragg grating spectrum prior to spin-coating.

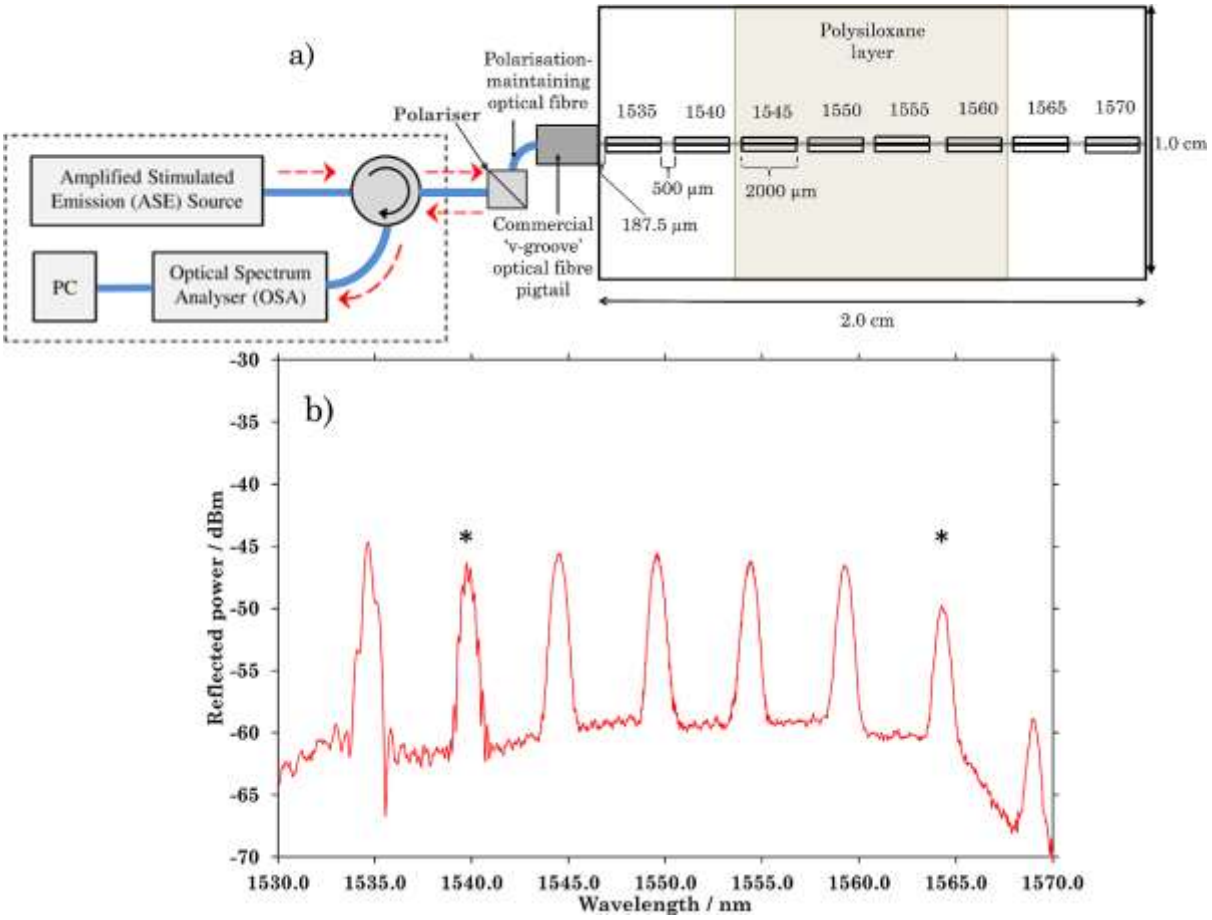

Fig.2: (a) No correlation is observed between the average Bragg wavelength shift of the uncovered Bragg gratings ($\Delta\lambda_{B(U)}$) and the refractive indices of the tested solvents. Propagated associated errors are represented by the *y*-axis error bars. **(b)** Comparison of the atmospheric temperature within the flow cell (thermocouple, black crosses) and the measured Bragg wavelength shift of the two uncovered Bragg gratings ($\Delta\lambda_{B(U)}$, red and blue lines) upon reversibly switching from dry nitrogen gas (N_2) to N_2 saturated with toluene vapour (pale blue shading), which became residual toluene vapour in N_2 (pale orange shading), and then switched back to dry N_2. The average temperature during the measurement was ~301 K and the proportion of toluene in saturated nitrogen was estimated as 4.3 %. The dashed line is a guide for the eye only.

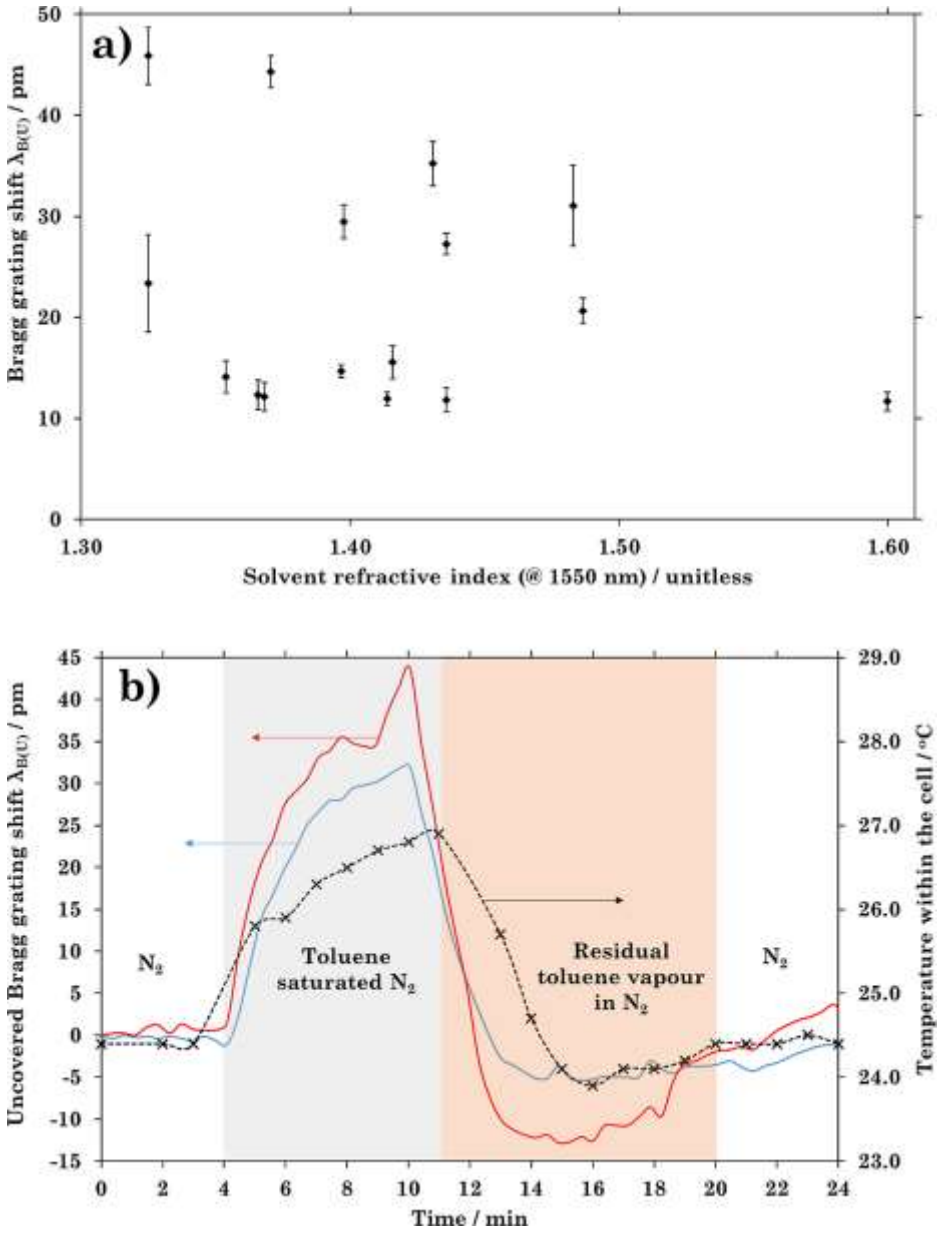

Fig.3: The relationship between $\delta(\Delta\lambda_B)$ and the refractive index (at ~1550 nm) of the solvents demonstrates a complex detection mechanism. The curved dashed black line is a guide for the eye only, with significant outliers carbon disulfide (CS_2) and water (H_2O) highlighted by red circles. The dashed red line designates $\delta(\Delta\lambda_B)$ = 0 pm. Propagated associated errors are indicated by the *y*-axis error bars.

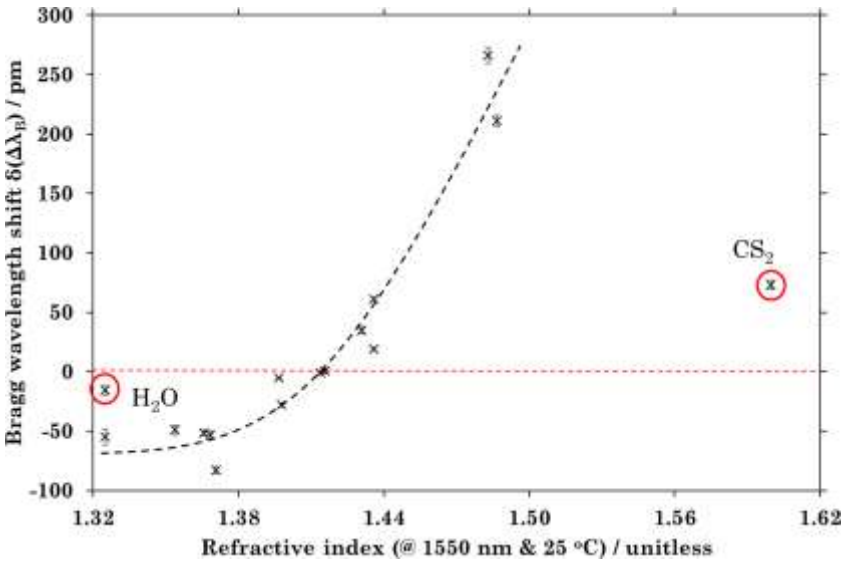

Fig.4: Relationship between the Hildebrand solubility parameter, δ_H, and $\delta(\Delta\lambda_B)$ for the solvents investigated, highlighting the asymptotic behaviour approaching $\delta_H \approx 18.5$ MPa$^{1/2}$ (shown by the thick blue line). The dashed black lines are guides for the eye only. The dashed red line denotes the position of $\delta(\Delta\lambda_B) = 0$ pm. Propagated associated errors are represented by the y-axis error bars and outliers are circled in red, with the solvent name given beside each outlier datum.

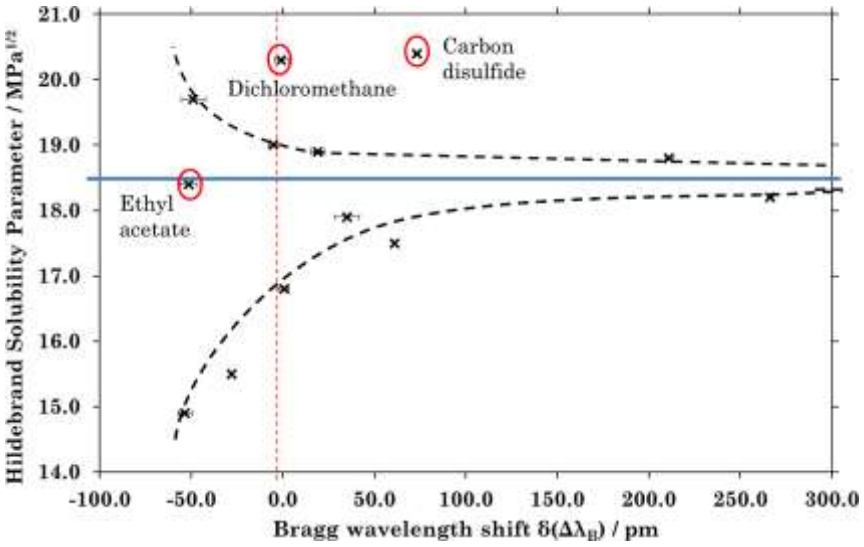

Fig.5: Correlation between the predicted Bragg wavelength shift for each solvent (calculated using **Eq.1)** and the corresponding measured Bragg wavelength shift. The training set is represented by black circles (•) while the solvents in the test set are marked by red circles (•). The vertical error bars represent the standard error, calculated from the regression model, of the predicted values and the horizontal error bars represent the associated errors in the experimental Bragg wavelength shift. The dashed line is a guide for the eye only.

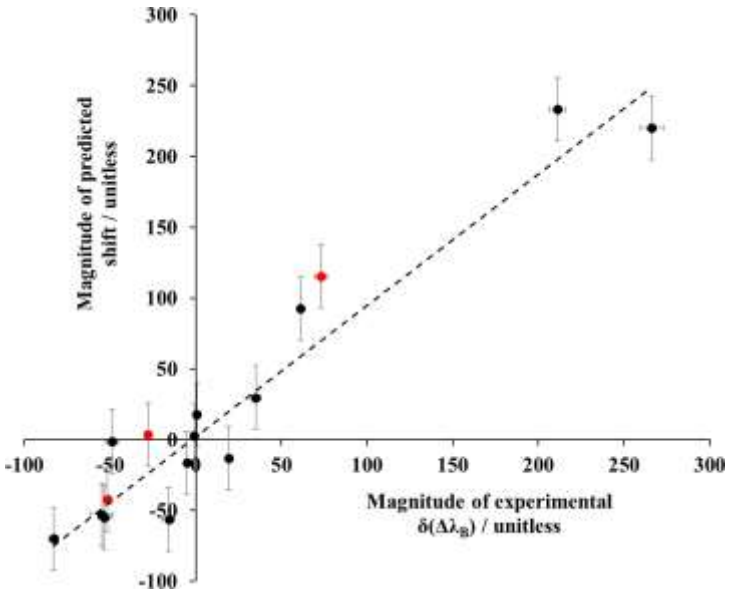

Fig.6: The determination of the response time of the sensor device during a switch from dry nitrogen gas to toluene vapour saturated nitrogen gas. The reflected spectrum, and consequentially the Bragg wavelength shift, $\lambda_{B(C)}$, was recorded at three second intervals and at a temperature of 301 K

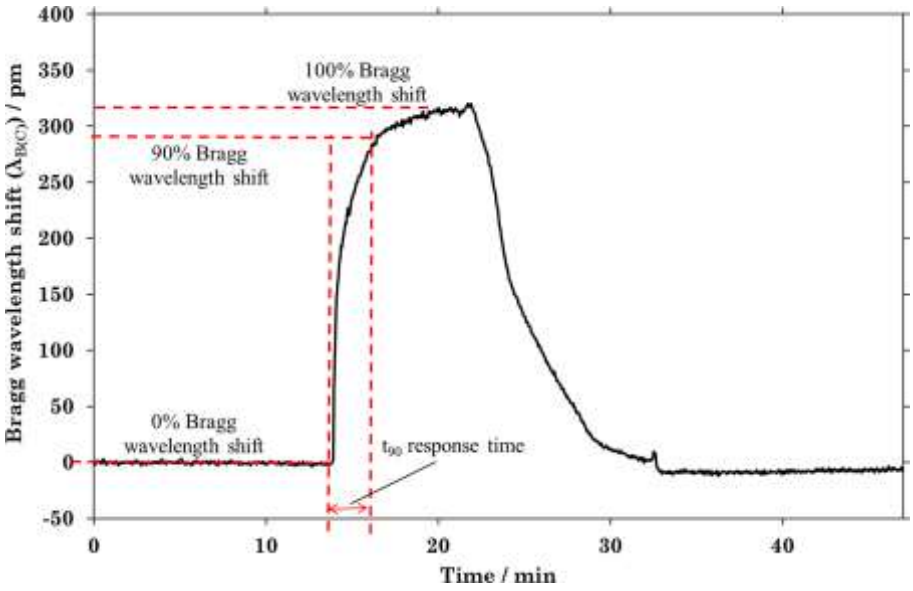

Table 1: List of the chemical descriptors investigated in the QSPR study.

Descriptor	Chemical Descriptor	Physico-chemical or theoretical property	Units	Description
1	Surface Tension	Physico-chemical	10^{-3} kg s^{-2}	The energy required to form an interface between the bulk solvent and the surrounding environment, usually the atmosphere. The value for each solvent was sourced from the literature [43–56].
2	Freezing point	Physico-chemical	K	The temperature at which the chemical changes state from a liquid to a solid [57].
3	Boiling point	Physico-chemical	K	The temperature at which the chemical changes state from a liquid to a gas [57].
4	Hildebrand Solubility Parameter	Physico-chemical	$MPa^{1/2}$ (10^6 Pa)	The square root of the cohesive energy density. The cohesive energy density describes the energy required to separate a unit volume of molecules to infinite separation from neighbouring molecules. Values were taken from the comprehensive work of Abboud and Notario [58], apart from oct-1-ene and 1,4-difluorobenzene which were calculated using **Eqn.S1** and literature values of ΔH_v [59,60].
5	Molecular Weight (MW)	Physico-chemical	g mol^{-1}	Relative molecular mass of the chemical. Calculated by hand.
6	Log_{10} K_{ow}	Physico-chemical	Unitless	A quantitative thermodynamic measure of the hydrophobic / hydrophilic behaviour of a chemical. The log_{10} K_{ow} values were taken from literature [61].
7	Refractive index (@ 1550 nm)	Physico-chemical	Unitless	The refractive index of the solvent at 1550 nm. Values were determined by taking n_D values (where n_D is the refractive index of a material at the sodium D-line wavelength) [38] and then converting these values into the refractive index at 1550 nm by use of Cauchy's equation; Cauchy's equation can be used to predict the refractive index of a material at a specific wavelength [62].
8	Topological Polar Surface Area (TPSA)	Theoretical property	$Å^2$ (10^{-10} m^2)	A measure of the polar surface area of a molecule. Values calculated using the Molinspiration online chemical descriptor tool [63].
9	Number of rotatable bonds	Theoretical property	Unitless	A topological parameter that describes molecular flexibility. A rotatable bond is defined as a single, non-ring bond to a non-terminal heteroatom. Values calculated using the Molinspiration online chemical descriptor tool [63].
10	Number of hydrogen bond donor groups	Theoretical property	Unitless	The number of –OH or –NH(R) groups within the molecule that are able to act as hydrogen bond donor groups. Counted/calculated by hand.
11	Number of hydrogen bond acceptor groups	Theoretical property	Unitless	The number of nitrogen atoms in the molecule substituted by a hydrogen or aliphatic chain or the number of oxygen atoms in the molecule that are bonded to a carbon atom by a double bond or substituted by a hydrogen or aliphatic chain. Oxygen atoms directly bonded to an atom, which is double bonded to another atom or oxygen atoms in an aromatic system are not counted. In this study, carbon disulfide, S=C=S, and 1,4-difluorobenzene were counted as possessing two H-bond acceptor groups each. The weak hydrogen bond acceptor behaviour of the C=S groups in carbon disulfide and the C-F bonds in 1,4-difluorbenzene has been reported [64,65].
12	Ring double bond equivalents (RDBE) value	Theoretical property	Unitless	The value gives an indication of the unsaturation of a molecule. The number gives the total sum of double bonds, rings and twice the number of triple bonds within a molecule. Values of descriptor (12) were calculated using **Eq.S2**, ESI.

Table.2: Values of the chemical descriptors, as defined in Table 1, for each of the solvents under investigation. Values of descriptor (12) were calculated using the following formula (Eqn.S2). The magnitude of the coefficients of variation for each of the descriptors is given in the final row, with the two smallest values highlighted in *red italics*.

	Descriptors											
Solvent	**1**	**2**	**3**	**4**	**5**	**6**	**7**	**8**	**9**	**10**	**11**	**12**
cyclohexane (CY)	0.02457	278.65	353.85	16.8	84.16	3.44	1.4158	0	0	0	0	1
ethyl acetate (EA)	0.02393	189.15	350.15	18.4	88.11	0.73	1.3658	26.31	2	0	2	1
benzene (Benz.)	0.02883	278.65	353.15	18.8	78.11	2.13	1.4865	0	0	0	0	4
chloroform ($CHCl_3$)	0.02656	210.15	334.15	18.9	119.38	1.97	1.4358	0	0	0	0	0
tetrahydrofuran (THF)	0.02704	165.15	339.15	19.0	72.11	0.46	1.3967	9.234	0	0	1	1
acetone (Acet.)	0.02280	179.15	329.15	19.7	58.08	-0.2	1.3538	17.07	0	0	1	1
cyclohexene (CH)	0.02588	169.15	356.15	17.5	82.143	2.86	1.4358	0	0	0	0	2
***n*-hexane (n-hex)**	0.01789	178.15	342.15	14.9	86.18	3.9	1.3682	0	3	0	0	0
dichloromethane (DCM)	0.02736	176.15	313.05	20.3	84.93	1.25	1.4138	0	0	0	0	0
carbon disulfide (CS_2)	0.03158	161.65	319.15	20.4	76.139	1.94	1.5997	0	0	0	2	2
isopropyl alcohol (IPA)	0.02119	183.65	355.15	23.7	60.1	0.05	1.3706	20.23	0	1	1	0
1,4-difluorobenzene (1,4-dfb)	0.02650	260.15	361.65	17.9	114.09	2.42	1.4308	0	0	0	2	4
oct-1-ene (O-1-E)	0.02120	172.15	395.65	15.5	112.24	4.57	1.3977	0	5	0	0	1
methanol (MeOH)	0.02260	175.15	337.85	29.7	32.04	-0.7	1.325	20.23	0	1	1	0
toluene (Tol.)	0.02794	180.15	383.65	18.2	92.14	2.73	1.4829	0	0	0	0	4
Coefficient of variation / %	**0.4698**	**0.2213**	***0.05396***	**0.1912**	**0.3778**	**1.047**	***0.03763***	**1.432**	**3.606**	**2.049**	**1.226**	**1.264**

Table 3: The correlation matrix for the ten chemical descriptors remaining. The correlations range from +1 to -1 inclusive, where -1 = perfect anti-correlation, 0 = no correlation and +1 = perfect correlation between the two descriptors. The red squares represent the cases where there is very significant anti–correlation or correlation (|0.70| < absolute magnitude of correlation coefficient). The chemical descriptors are as labelled as defined in Table 1.

Descriptor	**1**	**2**	**4**	**5**	**6**	**8**	**9**	**10**	**11**	**12**
1		0.47726	0.24645	-0.51682	-0.37424	0.52293	-0.23881	0.72501	0.17664	-0.09813
2	0.47726		-0.12432	0.01700	0.16838	-0.02800	-0.19636	0.20665	0.10598	0.32451
4	0.24645	-0.12432		-0.71320	-0.83297	0.76011	-0.39584	0.72008	0.39760	-0.37701
5	-0.51682	0.01700	-0.71320		0.74075	-0.88427	0.11250	-0.80541	-0.26528	0.41105
6	-0.37424	0.16838	-0.83297	0.74075		-0.87768	0.45396	-0.66145	-0.54239	0.40872
8	0.52293	-0.02800	0.76011	-0.88427	-0.87768		-0.20985	0.86796	0.52893	-0.47333
9	-0.23881	-0.19636	-0.39584	0.11250	0.45395	-0.20985		-0.14665	-0.24505	-0.23777
10	0.72509	0.20665	0.72008	-0.80541	-0.66145	0.86796	-0.14665		0.36962	-0.41842
11	0.17664	0.10598	0.39760	-0.26528	-0.54239	0.52893	-0.24505	0.36962		0.06463
12	-0.09813	0.32451	-0.37701	0.41105	0.40872 1	-0.47333	-0.23777	-0.41842	0.06463	